Geomechanics and Engineering, *Vol. 30, No. 1 (2022) 27-44*
https://doi.org/10.12989/gae.2022.30.1.027

Mechanical properties and failure mechanism of gravelly soils in large scale direct shear test using DEM

Yiliang Tu*[1,2,3,4], Xingchi Wang[2], Yuzhou Lan[2], Junbao Wang[4] and Qian Liao[1]

[1]*State Key Laboratory of Mountain Bridge and Tunnel Engineering, Chongqing Jiaotong University, Chongqing 400074, China*
[2]*School of Civil Engineering, Chongqing Jiaotong University, Chongqing 400074, China*
[3]*China Merchants Chongqing Communications Research & Design Institute Co., Ltd., Chongqing 400067, China*
[4]*Shaanxi Key Laboratory of Geotechnical and Underground Space Engineering, Xian University of Architecture and Technology, Xi'an 710055, China*

(Received July 31, 2021, Revised May 10, 2022, Accepted May 13, 2022)

Abstract. Gravelly soil is a kind of special geotechnical material, which is widely used in the subgrade engineering of railway, highway and airport. Its mechanical properties are very complex, and will greatly influence the stability of subgrade engineering. To investigate the mechanical properties and failure mechanism of gravelly soils, this paper introduced and verified a new discrete element method (DEM) of gravelly soils in large scale direct shear test, which considers the actual shape and broken characteristics of gravels. Then, the stress and strain characteristics, particle interaction, particle contact force, crack development and energy conversion in gravelly soils during the shear process were analyzed using this method. Moreover, the effects of gravel content (GC) on the mechanical properties and failure characteristics were discussed. The results reveal that as GC increases, the shear stress becomes more fluctuating, the peak shear stress increases, the volumetric strain tends to dilate, the average particle contact force increases, the cumulative number of cracks increases, and the shear failure plane becomes coarser. Higher GC will change the friction angle with a trend of "stability", "increase", and "stability". Differently, it affects the cohesion with a law of "increase", "stability" and "increase".

Keywords: damage evolution; direct shear test; gravelly soils; numerical simulation

1. Introduction

Widely distributed in nature, gravelly soils are composed of a soil matrix of fine particles mixed with gravel particles, which is a kind of special geotechnical material and often used to fill subgrade engineering in the construction of railway, highway and airport (Coli *et al*. 2012, Chang *et al*. 2014, Chang and Phantachang 2016a, Song *et al*. 2018, Chang and Chou 2019). The mechanical properties of gravelly soils from different sites are quite different (Lindquist 1994, Medley 1994, Eliadorani *et al*. 2005, Kalender *et al*. 2014). It is quite important to conduct a research on the mechanical properties of S-RM, which significantly affect the stability of subgrade engineering.

Up to now, many geotechnical tests were conducted to study the shear mechanical properties of gravelly soils such as in-situ test, large-scale direct shear test, triaxial compression test, etc. (Sonmez 2006, 2016, Chang *et al.* 2021). Zhang *et al*. (2016) studied the strength and deformation properties of gravelly soils by large-scale in-situ test. Chang and Phantachang (2016a) investigated the effects of gravel content (GC) on the shearing characteristics of gravelly soils using a series of drained simple shear tests. Xu *et al*. (2011) studied the influence of maximum particle size, gradation, water content and GC of gravelly soils on shear strength and failure mechanism of slope through direct shear tests. Wang *et al*. (2018) investigated the meso-scale mechanisms which result in damage evolution in gravelly soils by a series of triaxial compression tests. Due to the limitation of laboratory test conditions, however, it is difficult to observe the failure characteristics of gravelly soils, particularly the failure evolution during shear process.

In recent years, the numerical analysis methods such as finite element method (FEM) and discrete element method (DEM) have been widely used in the study of gravelly soils. Li *et al*. (2016) used FEM to simulate direct shear test of gravelly soils. It is found that the gravel particle will greatly affect the stress distribution and failure mode of gravelly soils. Cen *et al*. (2017) found that under direct shear condition, the fracture surface of gravelly soils is irregular which is caused by the shear stress. Afifipour and Moarefvand (2014a, b) adopted FEM to study the failure mechanism of gravelly soils under uniaxial compression. Li *et al.* (2016) conducted triaxial compression tests by FEM and found that the cracks usually first appear at the interface between soil and gravel where shear stress is easy to accumulate.

Since gravelly soils are heterogeneous and discontinuous, and FEM is limited in simulating large deformation, fracture and rotation of particles, the simulation results of gravelly soils by FEM are different

*Corresponding author, Associate professor
E-mail: tyl_ok@126.com

ISSN: 2005-307X (Print), 2092-6219 (Online)

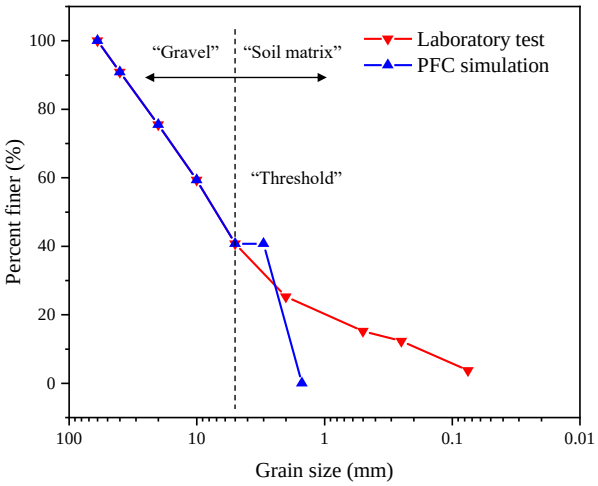

Fig. 1 The grain size distributions of gravelly soils in laboratory test and numerical test

from those of laboratory test (Tsoungui *et al*. 1999, Ben and Einav 2010, Chang *et al*. 2016b, Jin *et al*. 2017, Kodicherla *et al*. 2019, Kamani and Ajalloeian 2020). DEM can exactly make up for these limitations of FEM, which is more suitable for the simulation of gravelly soils and has been widely used in recent years. Graziani *et al*. (2012) simulated different shapes of the gravel particles, i.e. circle, triangle, rectangle and rhombus to conduct shear test and studied the relationship between gravel particle shape and micro-mechanical properties. A series of regular polygon models were built to simulate gravel particles in shear tests by Jin *et al*. (2017). The research shows that GC plays an important role for the mechanical properties of gravelly soils (Jin *et al*. 2017, Zhou *et al*. 2018). Xu *et al*. (2019) set up sphere models for gravel particles to carry out numerical shear test. It is found that when GC is 60%, the shear strength, friction angle and maximum dilatancy rate of gravelly soils all reach the maximum.

Although the shape of gravel particles is simulated in the numerical experiments, it is still quite different from actual ones. However, the shape irregularity of gravel particles has a great influence on the mechanical behavior of gravelly soils (Shinohara *et al*. 2000, Cho *et al*. 2007, Katagiri *et al*. 2010, Chang *et al*. 2014). If the actual shape of gravel particles is ignored in numerical test, larger deviation may occur as a result. Fine modeling is thus significant for simulating gravelly soils. Based on a circle model, Cen *et al.* (2017) used random polygons to simulate gravel particles and conduct shear tests, finding that the rotation angle of gravel particles in shear band is much larger than that in other places. Xu *et al*. (2015) adopted a method of non-overlapping assemblage to simulate convex polyhedral gravel particles. It shows that rotation and overcoming of the occlusion of the larger gravel particles in the localization band are more difficult than small soil particle, meanwhile localization characteristics and contact force distribution are affected by gravel.

Because the shapes of gravel particles in two dimensions can be concave or convex, it is necessary to improve the convex polygon modeling method of gravel particles in the above literature into a method which can simulate both concave and convex polygons. Besides, in the studies of Cen *et al*. (2017) and Huang *et al*. (2017), rigid clumps which can't be broken were used to simulate gravel particles. In fact, the gravel particles in gravelly soils may be broken under compression or shearing (Hardin 1985, Indraratna and Salim 2002, Einav 2007, Indraratna *et al*. 2012, Shahnazari and Rezvani 2013, Rahmani and Panah 2020, Tu *et al*. 2021). Lobo-Guerrero and Vallejo (2005) studied the breakage development of particles in direct shear tests and found that particle breakage reduces the friction coefficient of the material. Through the direct shear test, Indraratna *et al*. (2012) found that particle breakage will lead to meso-structure rearrangement of gravelly soils and the increasing of sample's density, which improves the shear strength of gravelly soils. Through several direct shear tests, Tu *et al*. (2021) found that gravels were broken during the shear process, resulting in the decrease of internal friction angle and the increase of cohesion. Therefore, in the numerical simulation of gravelly soils, it is necessary to consider the breakage of gravel particles.

This paper aims to establish a new DEM for gravelly soils and investigate their shear mechanical properties and failure mechanism in large scale direct shear tests. Compared with the traditional methods, the new method adopts random polygon (both convex polygon and concave polygon) to simulate gravel particles, and allows the possibility of breakage in gravel particles, which is more consistent with the actual gravel particles. Then, the numerical models of gravelly soils in large scale direct shear tests are established and loaded to failure. The reliability of this method is verified by comparing the results of numerical tests and laboratory tests. Finally, the mechanical properties and failure mechanism of gravelly soils during the shear process are analyzed, and their influence by GC are discussed.

2. Laboratory direct shear test for gravelly soils

In this paper, 5 mm is used as a threshold between soil matrix and gravel particles (Zhang 2015, Zhang *et al*. 2015). Several laboratory large scale direct shear tests for gravelly soils were conducted to obtain its macro-mechanical behavior in this study. Gravelly soils used in the

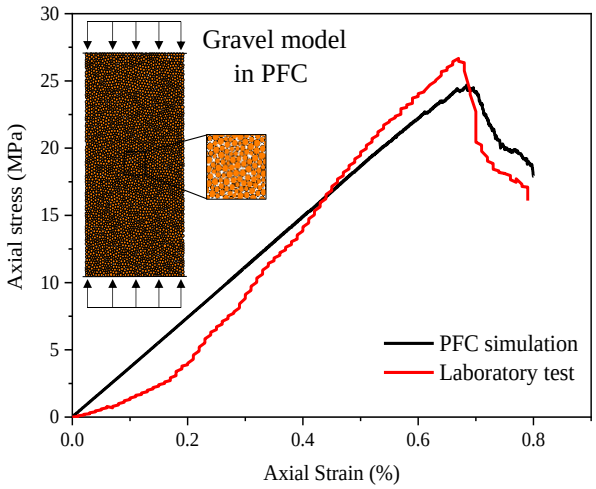

Fig. 2 The axial stress-strain curves of a column of gravel obtained from the laboratory and numerical uniaxial compression tests

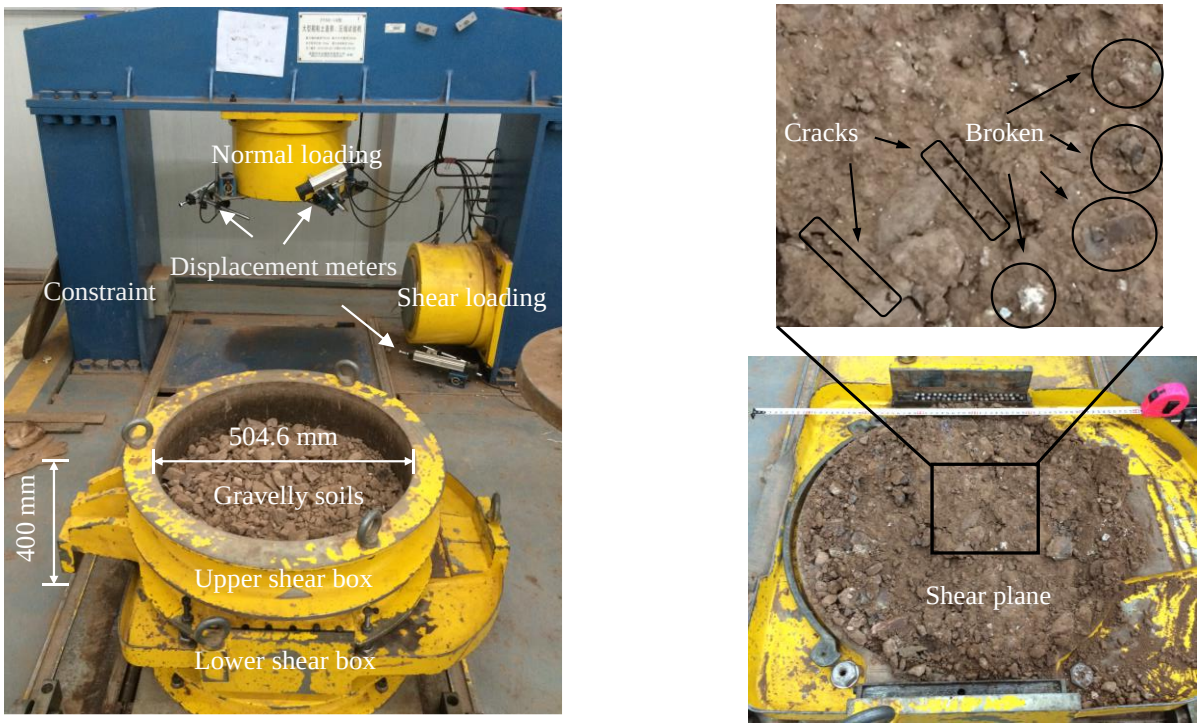

(a) Test apparatus (b) a typical failure sample (σ_n=600 kPa)

Fig. 3 Laboratory large scale direct shear test for gravelly soils

test were taken from Yubei District, Chongqing, China. The grain size distribution is shown in Fig. 1. According to the Unified Soil Classification System (USCS), the gravelly soils are classified as poorly graded gravel with sand (GP). GC, dry density, natural void ratio and water content of the gravelly soils are 59%, 1.9g/cm^3, 0.35 and 9.2%, respectively. The lithology of gravel with particle size greater than 5 mm is argillaceous sandstone. The axial stress-strain curve of a column of gravel with a diameter of 50 mm and a height of 100 mm was obtained through an uniaxial compression test, as shown in Fig. 2. The curve shows that the uniaxial compressive strength and elastic modulus of the gravel are 26.67 MPa and 3.53 GPa, respectively. The soil matrix with particle size less than 5mm contains 9.21% clay and 16.2% water, which is in the state of unsaturation. Through the direct shear test, the cohesion and friction angle of the soil matrix is evaluated as 60.6 kPa and 17.8°, respectively.

A large scale direct shear test apparatus with a shear box of diameter of 504.6 mm and height of 400 mm was used in the laboratory test, as shown in Fig. 3(a). The lower half of shear box was pushed with a horizontal velocity of 1.33×10$^-$

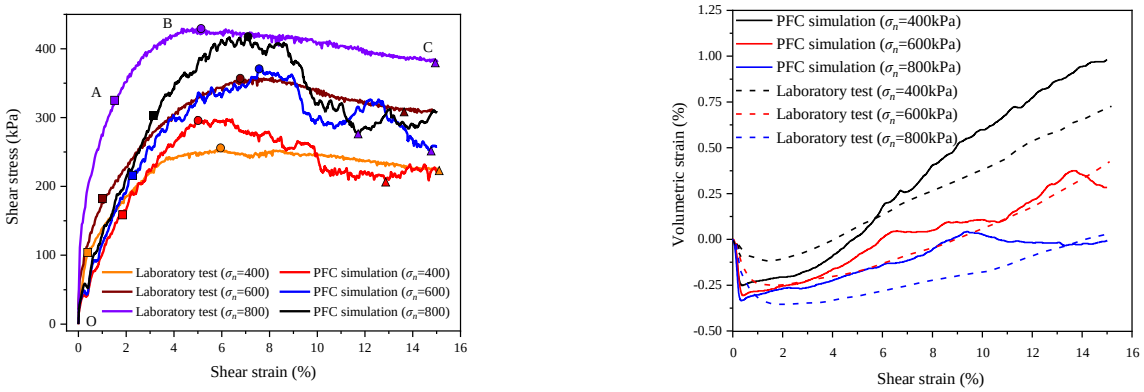

(a) Shear stress-strain curves (b) Volumetric strain-shear strain curves

Fig. 4 Stress and strain characteristics of gravelly soils with GC of 59% obtained from the laboratory and numerical tests.

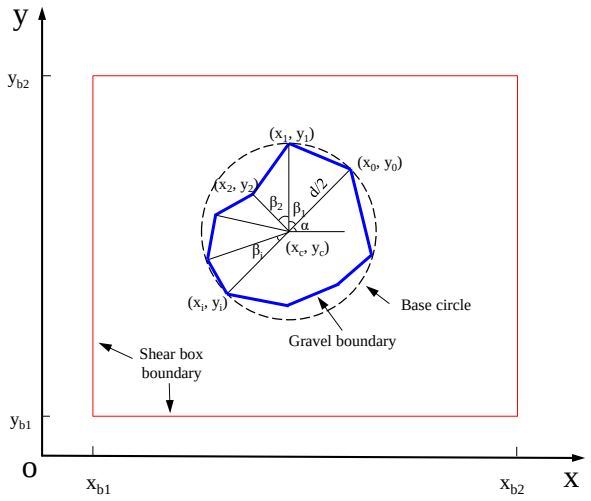

Fig. 5 Random polygon simulation method for breakable gravel

[5] m/s to realize shear deformation under constant normal stresses (σ_n) of 400, 600, or 800 kPa. Fig. 3(b) shows a typical shear plane of the damaged gravelly soils in shear test under normal stress of 600 kPa. It can be found that some cracks appear on the shear plane and the gravel particles are obviously broken.

The shear stress (τ) was defined as the horizontal force divided by the cross section area of sample. The shear strain (γ) was calculated as the horizontal displacement divided by the height of sample (Chang and Phantachang 2016a, Xu *et al.* 2016). The volumetric strain was evaluated as the normal displacement divided by the height of sample. Fig. 4 (a) shows the shear stress–strain curves for gravelly soils with GC of 59% obtained from laboratory tests. The shapes of the three curves are similar and can be divided into three typical stages: rapid stress rise stage (OA), yield stage (AB), residual stress stage (BC). The shear stress reach the peak at point A and then drop to residual stress at point C. Fig. 4(b) shows the volumetric strain-shear strain curves for gravelly soils with GC of 59% obtained from laboratory tests. If the volumetric strain is greater than zero, it indicates the shear dilation, or otherwise contraction. The results show that under normal stress of 400 kPa, the sample is contracted at small shear strain and then turns to be dilated when the shear strain exceeds 4%. The increasing normal stress causes the contraction of the gravelly soils to increase, which is a common phenomenon in geotechnical tests (Xu *et al.* 2011, Indraratna *et al.* 2014, Gong *et al.* 2019). The development of volumetric strain is related to the climbing of particles in the vertical direction during the shearing process (Chang and Phantachang 2016a). When the shear strain or normal stress increases, the vertical climbing displacement among particles will increase.

3. A new DEM of gravelly soils in large scale direct shear test

3.1 Random polygon simulation method for breakable gravel particle

Cen *et al.* (2017) introduced a method to build numerical model of gravelly soils with random structure using PFC^{2D}. However, this method can't simulate the breakage and concave polygon shape of gravel particle. This paper will improve it and introduce a random polygon simulation

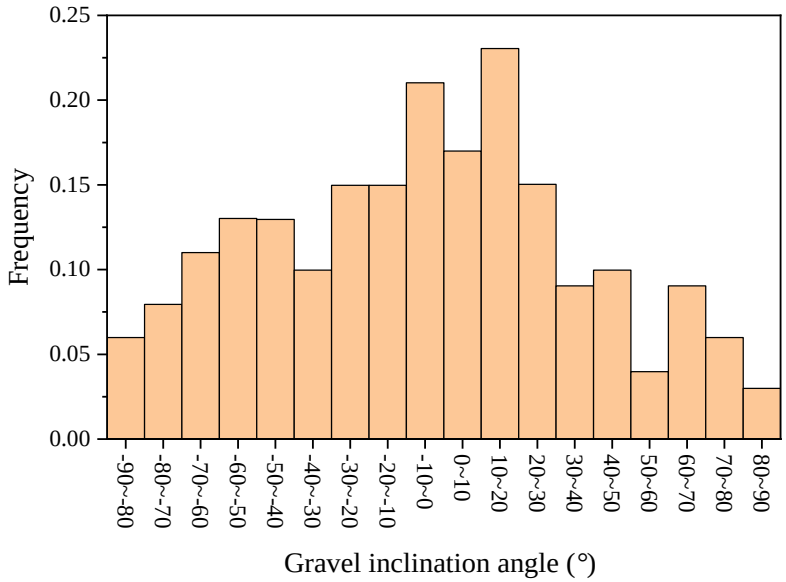

Fig. 6 Gravel directional frequency distribution (Cen *et al.* 2017)

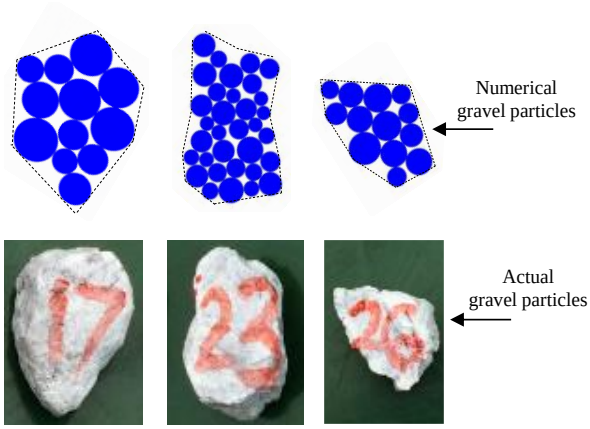

Fig. 7 Gravel models using random polygon simulation method in PFC

method for breakable gravel particle, as shown in Fig. 5.

3.1.1 Gravel particle size

Assuming that the size distribution of gravel particles in any grain group is uniform, the diameter of gravel particles can be randomly generated according to Eq. (1)

$$d = d_{min} + urand \times (d_{max} - d_{min}) \tag{1}$$

where d is the diameter of gravel particles; d_{max} and d_{min} are the largest and smallest particle size in a certain group, respectively; *urand* is a random number with uniform distribution [0, 1].

3.1.2 Position of gravel particle

Assuming that the probability of gravel particle appearing at any position in the shear box is the same, the location of gravel particle in gravelly soils model can be determined randomly according to Eq. (2).

$$\begin{cases} x_c = x_{b1} + uranb \times (x_{b2} - x_{b1}) \\ y_c = y_{b1} + uranb \times (y_{b2} - y_{b1}) \end{cases} \tag{2}$$

where, x_c and y_c are the center coordinates of the base circle which is connected with the long axis of the gravel particle; x_{b1}, x_{b2}, y_{b1}, y_{b2} represent model boundaries, i.e., shear box.

3.1.3 Inclination angle of gravel particle

The inclination angle α is defined as the included angle between the horizontal direction and the long axis of gravel particle (diameter of the basic circle). When the included angle is greater than 90°, the inclination angle equals to the included angle minus 180°. Cen *et al*. (2017) made statistics on the inclination angle of gravel particle in gravelly soils fill, and found that it follows the law shown in Fig. 6. This result is introduced in this study to determine the inclination angle α gravel particle.

3.1.4 The number of gravel particle sides

The accuracy of the numerical model for gravel particle increases with an increment in its side number, while it calls for higher calculation ability of the computer. This simulation method balances the model accuracy and the

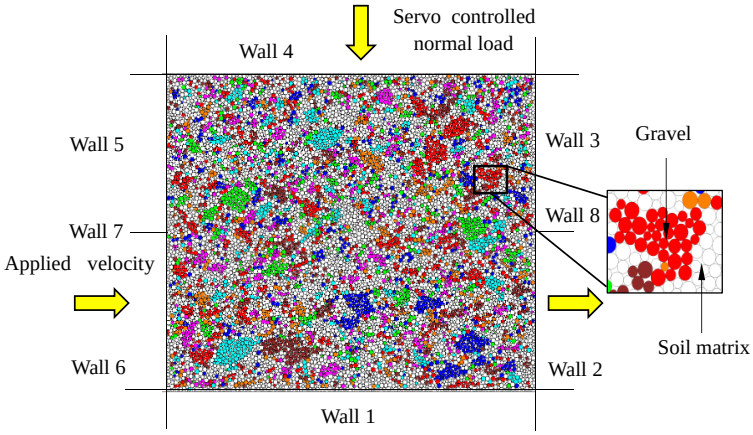

Fig. 8 Numerical model of gravelly soils in large scale direct shear test

computational efficiency to take side number n as an integer following the uniform distribution from 8 to 16 (see Eq. (3))

$$n = int(8 + urand \times 8) \tag{3}$$

3.1.5 The concavity and convexity of gravel particle

The concavity and convexity of gravel particle can be judged by the internal angles corresponding to each vertex i of gravel particle. As long as there is an internal angle which is greater than 180°, it is a concave polygon, otherwise it is a convex polygon, as shown in Fig. 5. On the basis of inclination angle α, rotate an angle β_i anticlockwise each time to determine the coordinates (x_i, y_i) of each vertex i. Thus, x_i and y_i can be calculated through Eq. (4)

$$\begin{cases} x_i = cos(\alpha + \sum \beta_i)\dfrac{d}{2}\eta_i + x_c \\ y_i = sin(\alpha + \sum \beta_i)\dfrac{d}{2}\eta_i + y_c \end{cases} \tag{4}$$

where, β_i is the angle between the adjacent vertices *i-1* and *i* of the polygon, which obeys [0, 180] uniform distribution, β_0=0; η_i is a random number that obeys [0, 1] uniform distribution.

3.1.6 The breakage of gravel particle

Fig. 3(b) shows that the gravel particles were seriously broken in the shear test. The crushing property of gravel particle should be considered in the numerical model. In PFC^{2D}, cluster is composed of several particles bonding together, which can move and rotate relatively to each other. Thus, cluster can be deformed and broken. If the magnitude of contact force exceeds the contact bond strength, the bond among particles will be broken, that is, cluster is broken (Bolton *et al*. 2008). Therefore, cluster is more accurate than the unbreakable clump to be used in the simulation of gravel particle.

Fig. 7 shows three models of gravel particles established by the above method. It can be seen that the numerical models are very similar to the actual gravel particles in shapes.

3.2 Numerical model of large scale direct shear test for gravelly soils

The size and boundary condition of shear box in numerical test is the same as those in the laboratory test. It is composed of 8 walls, as shown in Fig. 8. During the shear test, the horizontal displacement of upper shearing box (wall 3-5) is fixed, a constant normal stress is applied on wall 4 using servo method, and the horizontal displacement of lower shear box (wall 1, 2, and 6) is set at a certain speed (i.e., loading speed).

It should be noticed that if the loading speed in PFC^{2D} is set to be the same as that in laboratory test (1.33×10^{-5} m/s), the calculation speed will be very slow. As a result, a sample needs to be loaded for months or even years. Therefore, it is inevitable to appropriately increase the loading speed. However, if the loading speed becomes too fast, it is difficult for the sample to maintain static equilibrium, and the numerical simulation results will be different from the laboratory test. Taking the calculation efficiency and the accuracy of the numerical results into consideration, a suitable loading speed should be set in PFC^{2D}. Many researchers have found that when the loading speed is set at about 0.05-0.1 m/s in PFC^{2D}, the requirements of calculation accuracy and calculation efficiency can be met at the same time (Bono and McDowell 2013, Bahaaddini 2017, Suhr *et al*. 2018). Therefore, the horizontal displacement of lower shear box (wall 1, 2, and 6) is set at a speed of 0.1 m/s.

According to the particle size distribution in Fig. 1, the gravel particles with size greater than 5mm is simulated by cluster using the method described in Section 3.1. The soil with particle size less than 5 mm is simulated by disc particles. It should be noted that in PFC simulation, the calculation efficiency decreases with the increases in the particle number. If the particle size in a model is set to be the same as the actual soil particle size, at least millions of particles need to be generated. It will make the numerical calculation program unable to run. The calculation efficiency is often improved by increasing the particle size in the model. However, if the particle size is too large (i.e. the number of particles is too small), the numerical test results will be quite different from the laboratory test. In order to balance the contradiction between the calculation efficiency and the accuracy of the calculation results, particles should be generated as much as possible within the

Table 1 Micro-parameters of soil matrix in PFC

Item	Value
Particle friction coefficient, u	0.6
Particle elasticity modulus, E_c (Pa)	7×10^6
Particle stiffness ration, k_n/k_s	10
Normal contact-bond strength, σ_{c-mean} (Pa)	1×10^5
Normal contact-bond strength, $\sigma_{c-std.dev.}$ (Pa)	1×10^4
Shear contact-bond strength, τ_{c-mean} (Pa)	8×10^5
Shear contact-bond strength, $\tau_{c-std.dev.}$ (Pa)	8×10^4

Table 2 Micro-parameters of gravel in PFC

Item	Value
Particle friction coefficient, u	0.6
Particle elasticity modulus, E_c (Pa)	1.75×10^7
Particle stiffness ration, k_n/k_s	2.5
Parallel-bond modulus, E_{pd} (Pa)	7.29×10^9
Parallel-bond stiffness ratio, k_{pb_n}/k_{pb_s}	1.2
Parallel-bond radius multiplier, pb_rad	0.3
Normal parallel-bond strength, σ_{c-mean} (Pa)	1.57×10^8
Normal parallel-bond strength, $\sigma_{c-std.dev.}$ (Pa)	3.14×10^7
Shear parallel-bond strength, τ_{c-mean} (Pa)	1.57×10^8
Shear parallel-bond strength, $\tau_{c-std.dev.}$ (Pa)	3.14×10^7

capacity of the computer. Therefore, in PFC, the maximum particle size is generally set to approximate the maximum particle size of the actual soil, and the ratio of the maximum and minimum particle sizes is as large as possible within the capacity of the computer. Some researchers have found that when this ratio exceeds 1.66, the numerical simulation results are in a good agreement with the laboratory test (Xu *et al*. 2016, Cen *et al*. 2017, Jiang *et al.* 2019, Kodicherla *et al.* 2019). In this study, the maximum diameter of soil particles is set to 3 mm and the ratio of the maximum and minimum particle sizes is 2.0. Consequently, a numerical model with 10770 disc particles and 2855 gravel clusters is generated to simulate the gravelly soils in large scale direct shear test, as shown in Fig. 8, where white particles represent soil matrix and colored clusters denote gravel particles. The grain size distribution of the gravelly soils in the model is shown in Fig. 1. Although the particle size distribution of soil matrix in the numerical model is different from that in laboratory test, the particle size distribution of gravel particles keeps consistent.

3.3 Contact constitutive models and parameter determination

The cohesion of soil matrix measured in the laboratory test is 60.6 kPa, indicating that there is bond strength among soil particles. In order to simulate the bond strength, the Contact-Bond Model (Liu *et al* 2015, Cen *et al* 2017) which can resist tension, shear and compression is adopted among the soil particles. It was observed that the gravel particles were crushed in the laboratory large scale direct shear test (see Fig. 3(b)). At present, the Parallel-Bond Model which can resist bending moment is widely used to simulate the fracture of rock (Xiao *et al.* 2017, Guo *et al.* 2020, Indraratna *et al.* 2020). Therefore, the Parallel-Bond Model is adopted in cluster for gravel particle. The Linear-Contact Model is generally used to define the contact between wall and soil or wall and gravel (Salazar *et al.* 2015, Chang *et al.* 2016b, Gong *et al.* 2019). The wall parameters have minor effects on the macro responses in the study of Chang *et al.* (2016b). The friction of walls is generally lower than that between particles (Hartl and Ooi 2011, Bono and Mcdowell 2013, Xu *et al* 2015, Zhang *et al* 2018, Danesh *et al*. 2020, Chen *et al*. 2021, Seyyedan *et al*, 2021). Thus, the friction coefficient on the walls is set at 0.3, and the normal and shear stiffness parameters between walls and balls are set to 10 times that between particles of soil matrix in this numerical test.

The accuracy of PFC^{2D} simulation results are highly related to the input micro-parameters. Up to now, there is no method to realize the transformation between material's macro-parameters and particle's micro-parameters. Consequently, "trial and error method" is often used for the determination of micro-parameters. With this method, the numerical tests are conducted through continuous adjustment of micro-parameters, until the numerical test results and laboratory test results are basically identical (Lee and Jeon 2011, Cen *et al*. 2017). This method is adopted in this paper. After hundreds of attempts, a group of micro-parameters for the gravelly soils are obtained, as

Table 3 The comparison of the peak shear stress obtained from laboratory tests and numerical tests (GC=59%)

Normal stress (kPa)	Peak shear stress (kPa)		Error rate (%)	Average error rate (%)
	Laboratory tests	numerical tests		
400	255.40	300.80	17.78	
600	358.10	370.97	3.59	8.02
800	430.80	419.17	2.70	

Table 4 The comparison of the strength parameters obtained from laboratory tests and numerical tests (GC=59%)

Strength parameters	Laboratory tests	PFC simulations	Error rate (%)
c (kPa)	85.00	105.81	20.81
φ (º)	23.68	22.81	3.67

shown in Tables 1 and 2. The numerical simulation results with this group of micro-parameters are shown in Figs 2 and 4 and Tables 3 and 4.

Fig. 2 shows the axial stress-strain curves of a column of gravel obtained from the numerical and laboratory uniaxial compression tests. The results show that the trends of the two curves are very similar except that the curve of numerical test shows more obvious "linearity" than that of laboratory test. The main reason for the difference is that there are some cracks and voids in the gravel sample tested in the laboratory. At the initial stage of loading (axial strain 0-0.2%), these cracks and voids should be compacted, resulting in the slow growth of the curve at this stage (Wang *et al.* 2020). However, in the numerical test, there are neither cracks in the gravel sample nor compaction space among particles because they are bonded together. This phenomenon has been reported by Jiang *et al.* (2017), Zhang *et al*. (2020) and Huang *et al*. (2022).

Fig. 4 shows the shear stress-strain curves and volumetric strain-shear strain curves of gravelly soils with GC of 59% obtained from the numerical and laboratory tests. The results show that the trends of the curves obtained by numerical tests are approximately consistent with that obtained by laboratory tests. Their main difference is that the roughness and fluctuation of the curves obtained by numerical tests are much larger, which can be attributed to two factors. The first factor is the particle number or particle size. The particle number of soil matrix in the numerical model is much smaller than that in the actual soil matrix. In other words, the particle size of soil matrix in the numerical model is significantly large, resulting in greater and more uneven instantaneous contact force among particles during loading (Cheng and Minh 2009, Kang *et al.* 2013, Ngo *et al.* 2016, Jing *et al.* 2020). Hence, the shear stress and volumetric strain in numerical tests are easy to increase or decrease rapidly. The second factor is the contact constitutive model among particles. In the numerical tests, the bonding strength is applied among particles using Contact-Bond Model and Parallel-Bond Model. When the bonds among particles are destroyed, Contact-Bond Model or Parallel-Bond Model will degenerate into Linear-Contact Model which can't resist tension and shear force. As a result, the bond strength among particles disappears, which leads to lower residual strength and greater fluctuation in the numerical test after the curves reach the peak stress. In the laboratory test, however, the bond strength among particles will not disappear completely

The comparison of the peak shear stress of GC of 59% obtained from laboratory tests and numerical tests is shown in Table 3, where the error rate is calculated as the difference is divided by the peak shear stress in laboratory tests. The results show that except for the error rate of 17.78% at 400 kPa normal stress, the other errors are within 5.00%. The average error rate is 8.02%, which is acceptable. The comparison of the strength parameters of GC of 59% obtained from laboratory tests and numerical tests is shown in Table 4. For the gravelly soils, the contribution of internal friction on shear strength is generally greater than cohesion, especially under high stress conditions. Although the error rate of cohesion (c) is 20.81%, the error rate of friction angle (φ) is 3.67%.

To sum up, although there are some differences between the numerical test results and laboratory test results in Figs 2 and 4 and Tables 3 and 4, the two results are generally consistent. It indicates that the new modeling method and the micro-parameters in Tables 1 and 2 are reliable, which can accurately describe the mechanical characteristics of gravelly soils.

4. Mechanical properties and failure mechanism of gravelly soils in direct shear test

4.1 Interaction among particles

Fig. 9 shows the interaction among particles in gravelly soils during shear process under normal stress of 600 kPa. Take the particles at position of "A", "B", "C" and "D" in the sample as examples to observe the typical modes of interaction. It can be seen that the interaction among particles is intense, including occlusion, sliding, climbing, rotation and breakage. The interaction among particles will affect the mechanical properties and failure characteristics of gravelly soils.

4.2 Contact force distribution

Fig. 10 shows the evolution of shear stress ratio, average contact force and contact force distribution of the sample with GC of 59% during shear process under normal stress of 600 kPa. The shear stress ratio is evaluated as the shear

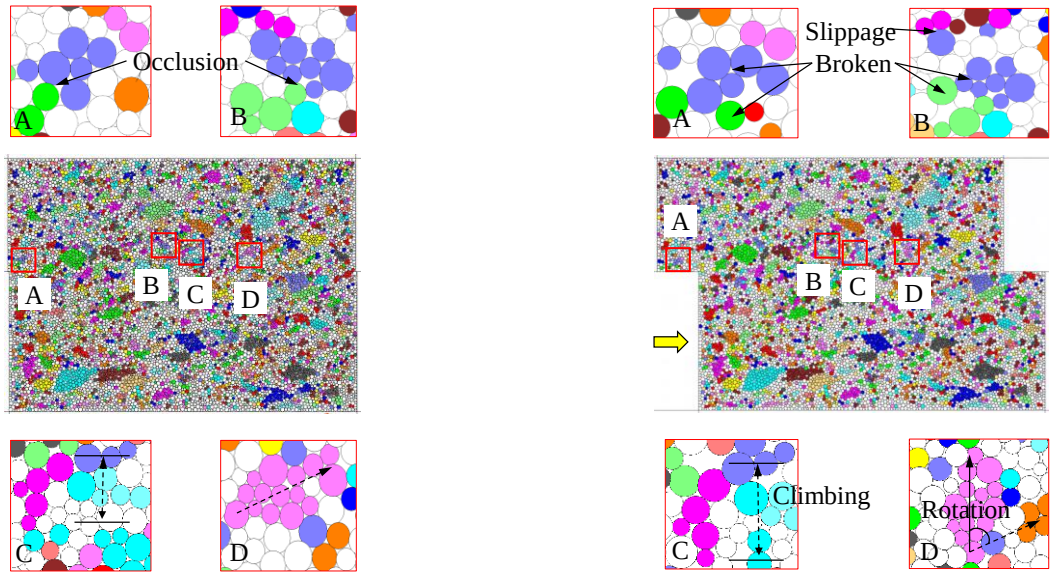

(a) shear strain=0.55% (b) shear strain=16.53%

Fig. 9 The interaction among particles in gravelly soils during shear process under normal stress of 600 kPa

stress is divided by normal stress. In the sample, the green clusters denote gravel particles, the black lines indicate the compressive forces, and the red lines represent the tensile forces. The line's direction and thickness indicate the direction and magnitude of contact force, respectively. Since the particles are mainly compressed, the tensile force is relatively small. Therefore, there are few tension chains in Fig. 10. It can be seen that the growing trend of average contact force is similar to that of shear stress ratio. The following phenomena can be found from Fig. 10.

- Before the sample is sheared, the shear stress ratio is 0 because the normal stress is applied only. The average contact force is small and the contact force lines are in circularly distributed. The contact force is almost uniformly distributed in the sample except for the stress concentration near some gravel particles.
- When the sample begins to be sheared, the particles squeeze into each other, resulting in an increment in the average contact force and the shear stress ratio. At this stage, the distribution of contact force becomes uneven and several strong force chains appear. The direction of the strong force chains is close to the normal stress and tilts about 16° against the shear direction. The principal stress becomes obvious and rotates against the shear direction.
- When the shear strain reaches 8%, the interaction among particles becomes more intense. Both the average contact force and the shear stress will reach the peak. At this point, the contact force distribution is very uneven and the strong force chain is mainly concentrated in the inclined area in the middle of the sample. The rotation angle of the principal stress or strong force chain reaches 60°.
- Compared with the previous stage, when the shear strain exceeds 8%, the contact force distribution changes little, but the average contact force and the number of strong force chains decrease gradually. The stress ratio begins to drop and enters the residual stress stage.

4.3 Crack development

Fig. 11 shows the crack development in gravelly soils with GC of 59% during shear process under normal stress of 600 kPa. When a bond contact in soil matrix or gravel particle is damaged, crack will appear at the corresponding position. The red lines represent the shear cracks and the black lines denote the tensile cracks. With the increase of shear strain, cracks in gravelly soils will develop into a shear plane. The following phenomena can be found in Fig. 11.

- When the shear strain is 0-2%, only a small number of cracks appear in the dislocation of the shear box (see point o-b in Fig. 11). This is mainly because the average contact force is relatively low as shown in Fig. 10. At this stage, partial tensile stress among several particles at the dislocation is generated because these particles have a tendency to separate from each other pushed by the horizontal force. The particles in other parts are denser after shearing.
- When the shear strain reaches 2-8%, many new cracks appear near the preset shear plane on the left side of upper shear box and right side of lower shear box (see point c-d in Fig. 11). The cumulative number of crack grow rapidly and its growth rate is maintained at a stable level. Based on the principle of breakage potential proposed by Hardin (1985), it is pointed out that although the average contact force increases rapidly, the breakage potential of particles decreases once it is crushed. As a result, the stress condition of particle breakage increases gradually, but the growth rate of crack number did not increase.
- When the shear strain is 8-12%, a shear band with a certain thickness is gradually generated in the sample (see point e in Fig. 11). The cumulative number of crack in gravelly soils keeps rising, while the growth rate of crack number begins to decrease. The reason for this

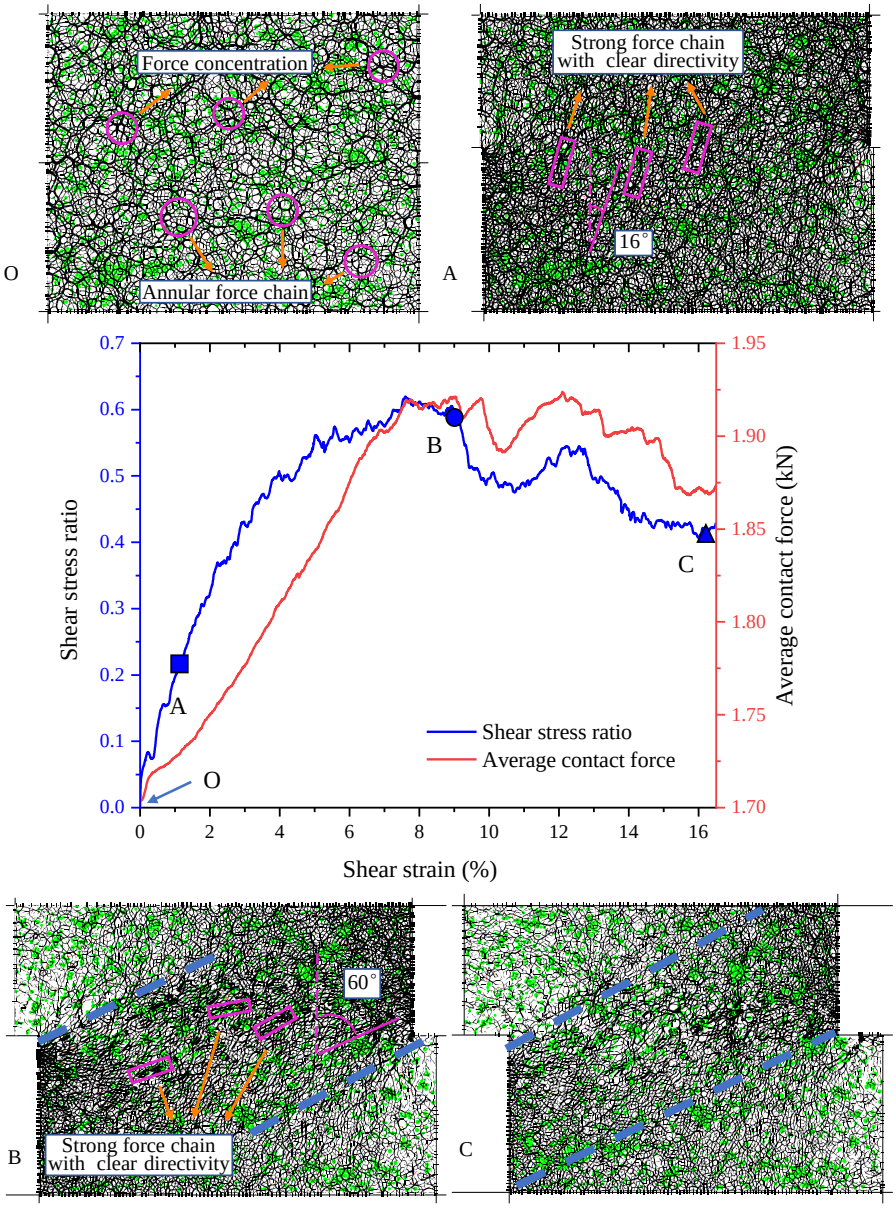

Fig. 10 The shear stress ratio, average contact force and contact force distribution of the sample with GC of 59% under normal stress of 600 kPa

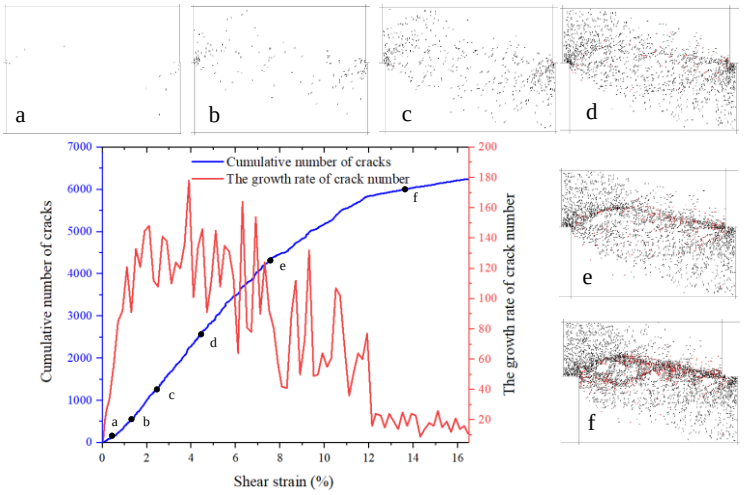

Fig. 11 The crack development in gravelly soils with GC of 59% under normal stress of 600 kPa

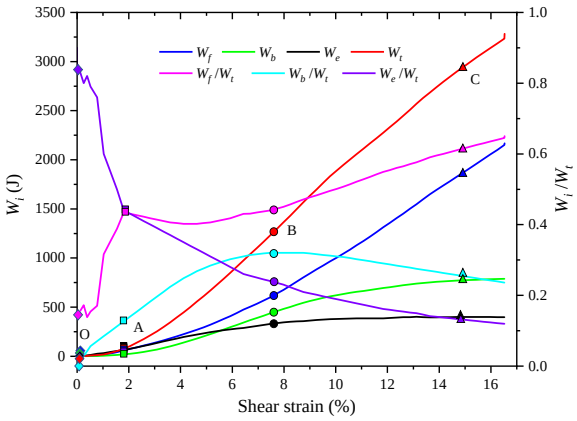

Fig. 12 The energy conversion in gravelly soils with GC of 59% under normal stress of 600 kPa (W_i is used to represent W_e, W_f, W_b and W_t)

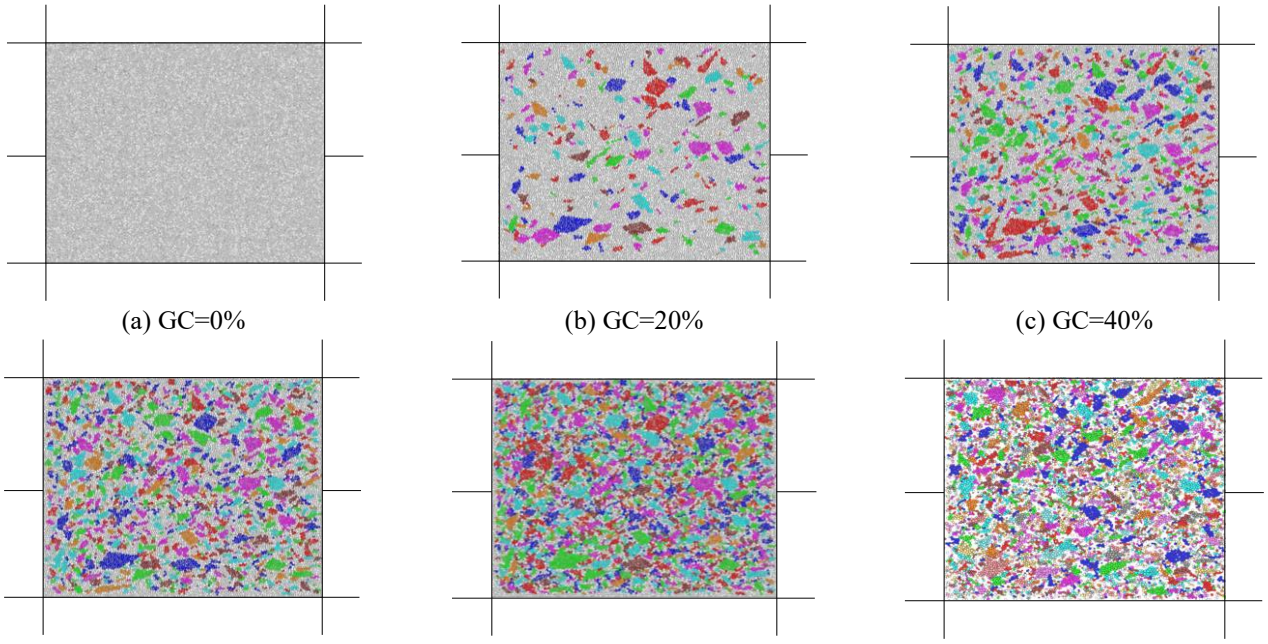

(a) GC=0% (b) GC=20% (c) GC=40%

(d) GC=59% (e) GC=80% (f) GC=100%

Fig. 13 The numerical models of gravelly soils with different GCs

phenomenon is that the average contact force and breakage potential are reduced at this stage, as shown in Fig. 10.

- When the shear strain exceeds 12%, a shear band penetrated by the cracks is formed, that is, the actual shear plane (see point f in Fig. 11). The cumulative number of cracks in gravelly soils is very small and the growth rate of crack number is close to zero. It is indicated that particle slip mainly occurs on the shear plane without breakage in gravelly soils at this stage. The sample is damaged and enters the stage of residual stress stage.

4.4 Energy conversion

Gravelly soil is a kind of complicated and discontinuous material. In the direct shear test, particle extrusion, deformation, slippage and breakage are accompanied by energy conversion. These sorts of energy follow the law of energy conservation. In detail they are the total energy (W_t) input by external load, the elastic strain energy (W_e) stored by particle deformation, the friction energy (W_f) consumed by particle friction, and the breakage energy (W_b) consumed by particle breakage. W_e/W_t, W_f/W_t and W_b/W_t are defined as the proportion of W_e, W_f and W_b in W_t, respectively. The conversion of these sorts of energy in gravelly soils with GC of 59% during shear process normal stress of 600 kPa is shown in Fig. 12. It can be seen that the energy conversion can be divided into three typical stages: approximately elastic deformation stage (OA), elastoplastic deformation stage (AB) and approximately plastic deformation stage (BC). Approximately elastic deformation stage (OA): although W_f/W_t and W_b/W_t are increase steadily, they are both less than 0.35. W_e increases rapidly, accounting for

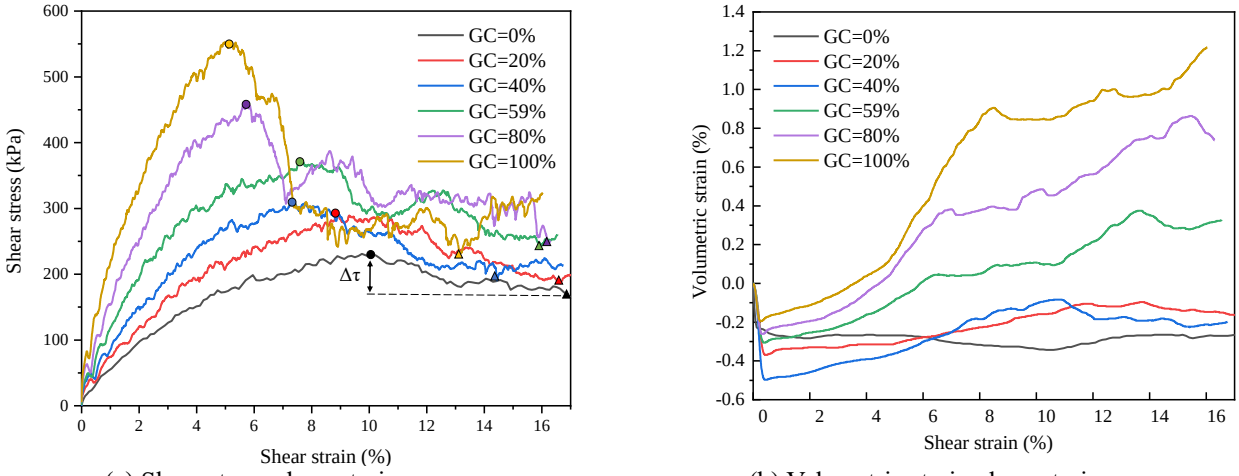

(a) Shear stress-shear strain curves (b) Volumetric strain-shear strain curves

Fig. 14 The stress and strain characteristics in the gravelly soils with different GCs under normal stress of 600 kPa

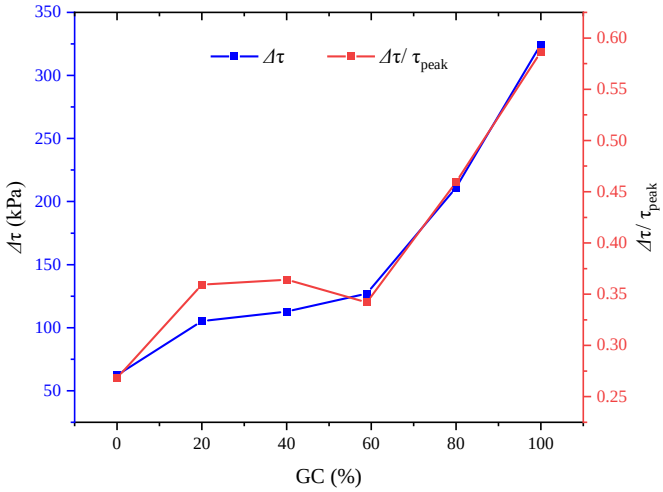

Fig. 15 $\Delta\tau$ and $\Delta\tau/\Delta\tau_{peak}$ in the gravelly soils with different GCs under normal stress of 600 kPa

more than 50% of W_t. At this stage, W_t is mainly converted into W_e, and the deformation of gravelly soils is mainly elastic deformation and shear densification.

Elastoplastic deformation stage (AB): the growth rate of W_e slows down and W_e/W_t decreases to 0.20-0.50. At the same time, both W_f and W_b increase rapidly, and their proportions in W_t increase to 0.45 and 0.25, respectively. The proportion of W_e, W_f and W_b in W_t is approximately equal, which indicates that neither the elastic deformation nor the plastic deformation can be ignored in this stage. At the end of this stage (shear strain is 87%), the shear stress (see Fig. 4) and the growth rate of particle breakage will reach the peak.

Approximately plastic deformation stage (BC): W_e increases slowly but its proportion in W_t decreases, accounting for about 10%-25%. W_b keeps growing, but W_b/W_t begins to decrease, which indicates that the growth rate of particle breakage slows down. It should be noted that W_f increase rapidly, resulting in W_f/W_t reaching 0.45-0.75. Thus, W_t is mainly converted into W_f, and the deformation of gravelly soils is mainly plastic deformation. At this stage, a shear plane is formed, and the sample in the shear box will slip along the shear plane.

5. Discussion

As an extremely important physical parameter of gravelly soils, GC will further affect strength, deformation and failure properties of gravelly soils by affecting the internal microstructural characteristics. Therefore, the influence of GC should be discussed. The numerical models of gravelly soils with different GC (0%, 20%, 40%, 59%, 80%, and 100%) are established in this paper, as shown in Fig. 13.

5.1 Effect of GC on stress and strain characteristics

Fig. 14 shows the shear stress-strain curves and volumetric strain-shear strain curves of the gravelly soil with different GCs under normal stress of 600 kPa. The trends of shear stress-strain curves of samples with different GCs are similar, which have experienced three stages: rapid

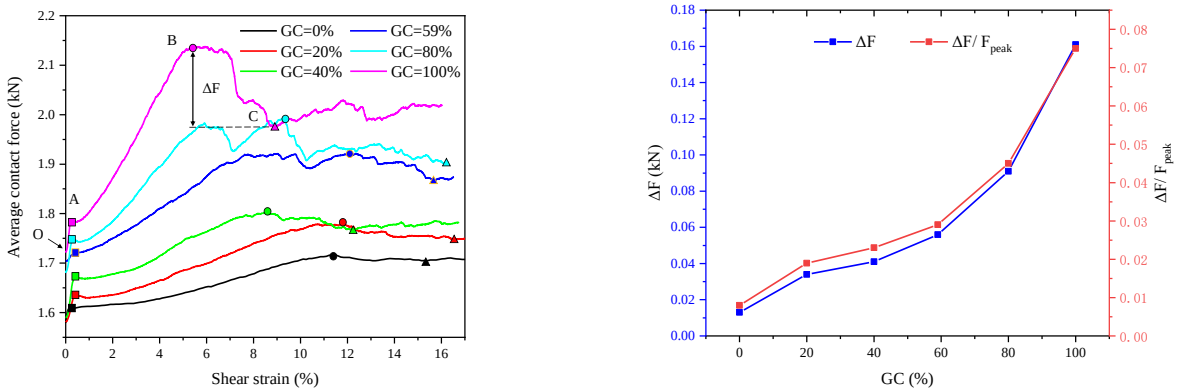

(a) The average particle contact force (b) ΔF and $\Delta F/\Delta F_{peak}$

Fig. 16 The particle contact force in the gravelly soils with different GCs under normal stress of 600 kPa

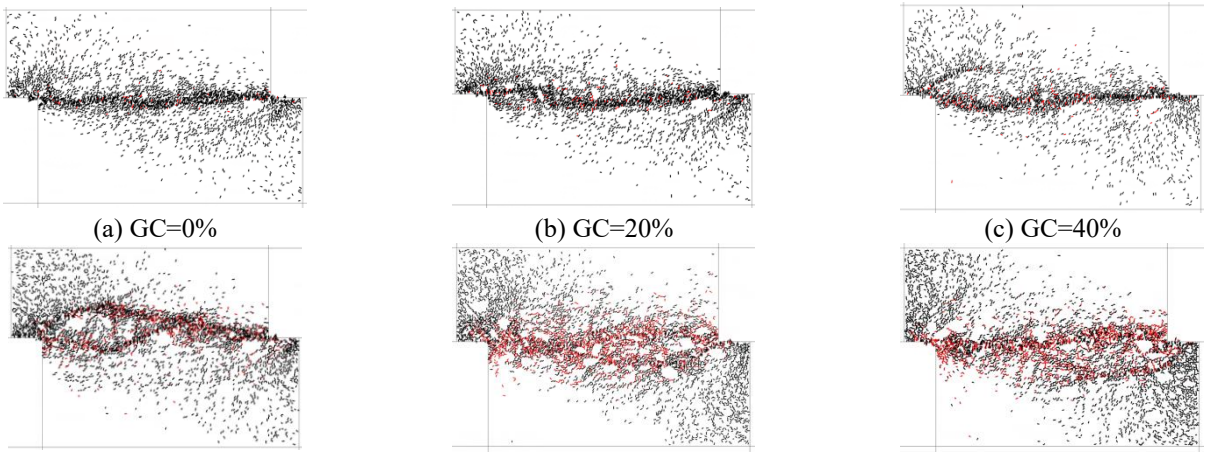

(a) GC=0% (b) GC=20% (c) GC=40%

(d) GC=59% (e) GC=80% (f) GC=100%

Fig. 17 Shear plane morphology of gravelly soils with different GCs under normal stress of 600 kPa

stress rise stage (OA), yield stage (AB) and residual stress stage (BC). Moreover, the shapes of the volumetric strain-shear strain curves with different GCs are similar, which first experience shear contraction and then gradually transform into shear dilation. Fig. 15 shows that both the value of the stress drop ($\Delta\tau$ in Fig. 14) from peak stress to residual stress and the ratio of $\Delta\tau$ to peak stress ($\Delta\tau/\Delta\tau_{peak}$) change with GC. The results show that GC has some significant effects on the shear stress and volumetric strain in Figs. 14 and 15, as follow:

With an increment in GC, the fluctuations of shear stress-strain curves become more significant due to stronger interactions among the gravel particles in the sample, which is consistent with the simulation results from Cen *et al*. (2017). The occlusion, squeeze and breakage of gravel particles lead to the accumulation and dissipation of strain energy, which increases and decreases the corresponding shear stress, respectively. Higher GC will aggravate the interaction among gravel particles.

With the increase in GC, the volumetric strain of the gravelly soils tends to dilate due to the intense climbing and overturning among the gravel particles in the sample. The climbing and overturning height of particles increases with the increase in GC.

Generally, $\Delta\tau$ and $\Delta\tau/\Delta\tau_{peak}$ increase with an increment in GC for the gravelly soils, which is not observed by Cen *et al*. (2017). This is attributed to the breakage of gravel, which will release the accumulated strain energy. Higher GC will aggravate the breakage of gravel particles and release more strain energy accumulated in gravelly soils.

5.2 Effect of GC on particle contact force

Fig. 16 shows that the average particle contact force, the value of the force drop (ΔF) from peak stress to average residual stress and the ratio of ΔF to peak stress ($\Delta F/\Delta F_{peak}$) all change with the GC under normal stress of 600 kPa. With the increase in GC, the average particle contact force increases gradually because the occlusion and stress concentration among particles are stronger in the sample with high GC (Fig. 16 (a)). ΔF and $\Delta F/\Delta F_{peak}$ increase with an increment in GC for the gravelly soils, which show the same change law as $\Delta\tau$ and $\Delta\tau/\Delta\tau_{peak}$ in Fig. 16. This is caused by particle breakage, which will reduce the average particle size of the sample. With the decrease of average particle size, the stress concentration and average contact force decrease, resulting in the drop of contact force. Higher GC will aggravate the breakage of gravel particles.

5.3 Effect of GC on morphological characteristics of shear plane

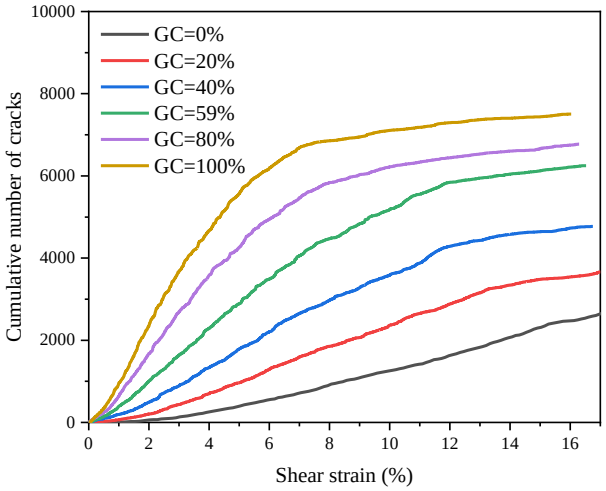

Fig. 18 The cumulative number of cracks in gravelly soils with different GCs under normal stress of 600 kPa

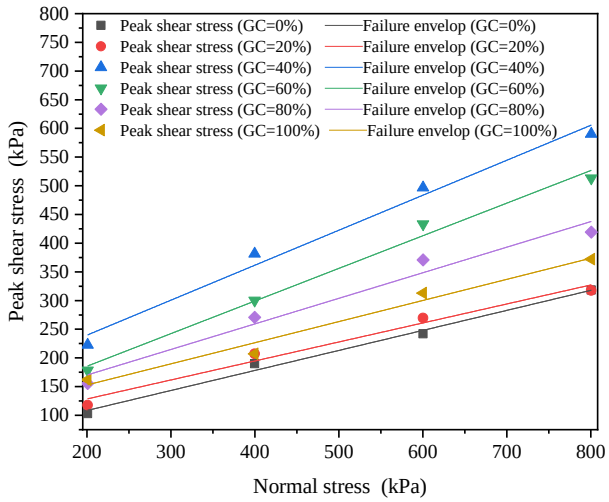

Fig. 19 Failure envelops of gravelly soils using Mohr-Coulomb strength criterion

Fig. 17 shows the shear planes in the damaged gravelly soils with different GCs under normal stress of 600 kPa. It can be seen that these shear planes do not develop completely in accordance with the preset plane. With the increase of GC, the shear planes fluctuate more wildly, that is, the shear plane become coarser. This indicates that GC has a great influence on shear plane morphology of gravelly soils. The extrusion, climbing and sliding among particles become intense with the increase of GC during the shear process.

5.4 Effect of GC on crack number

Fig. 18 shows the cumulative number of cracks in gravelly soils with different GCs during the shear process under normal stress of 600 kPa. It can be seen that the growing trends of the crack number with each GC are similar. On the whole, it follows the trend of "none" – "slow" – "fast" – "slow" – "stable". The sample with higher GC has higher contact force, thicker shear band and greater particle breakage rate. As a result, the cumulative number of cracks will increases with an increment in GC.

5.5 Effect of GC on shear strength parameters

The variation of the peak shear stress of gravelly soils with different GCs under different normal stresses is shown in Fig. 19. It can be found that the peak shear stress increases with an increment in GC. This is attributed to the structural effect produced by occlusion among the gravel particles. In detail, the overturning, sliding and crushing of gravel particles in gravelly soils with high GC are more intense.

The Mohr-Coulomb strength criterion is used to fit the test data in Fig. 19. The fitting correlation coefficients of M-C strength criterion are all above 0.97, indicating that gravelly soils within 200~800 kPa normal stress meets the criterion. Consequently, cohesion (c) and friction angle (φ)

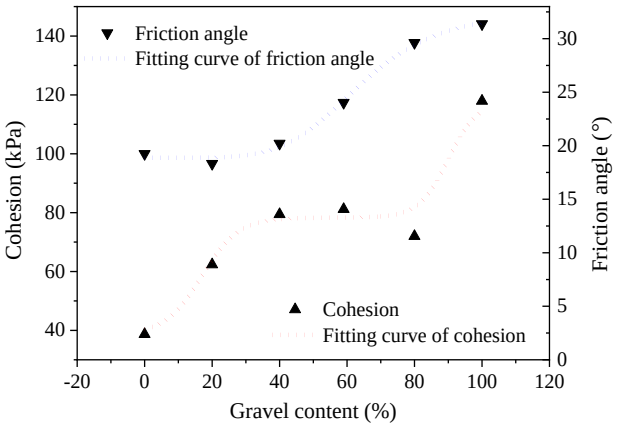

Fig. 20 Effect of GC on shear strength parameters of gravelly soils

of the gravelly soils can be calculated, as shown in Fig. 20. It appears that GC has a significant effect on shear strength parameters.

5.5.1 Effect of GC on friction angle

Fig. 20 shows that with the increase of GC, the friction angle φ has experienced three stages of "increase", "stability" and "increase". It satisfies the Eq. (5)

$$\varphi = \frac{\varphi_1 - \varphi_2}{1 + (GC/GC_0)^k} + \varphi_2 \tag{5}$$

where, φ_1 and φ_2 are the friction angle when GC is 100% and 0%, respectively, φ_1=32.68°, φ_2=18.87°. GC_0 is the characteristic GC, indicating the inflection point of the growth curve, and GC_0= 64.23%; k is the growth curvature coefficient, indicating the effective influence range of GC, and k= 5.33.

The internal friction of gravelly soils is mainly composed of sliding friction and occlusion friction among the particles. When GC is less than 20%, there is no effective contact among the gravel particles that the friction mainly comes from sliding friction, and the friction angle increases slowly. When GC is 20%-80%, the effective contacts among gravel particles increase gradually, which makes the occlusion friction increase. As a result, the friction angle increases rapidly. When GC is more than 80%, gravel particles are distributed throughout the gravelly soils, resulting in no more growth space for occlusion friction. Therefore, the growth rate of friction angle gradually slows down.

5.5.2 Effect of GC on cohesion

It can be seen from Fig. 20 that the change of cohesion c with GC can be divided into three stages ("growing"-"stable"-"growing"), which satisfies the Eq. (6)

$$c = c_1 + (c_2 - c_1) \cdot \left[\frac{0.5}{1 + 10^{(GC_1 - GC)h_1}} + \frac{0.5}{1 + 10^{(GC_2 - GC)h_2}} \right] \tag{6}$$

where, c_1 and c_2 are the friction angle when GC is 0% and 100%, respectively, and c_1=32.68 kPa, c_2=18.87 kPa; h_1 and h_2 are growth rate parameters, and h_1=0.08, h_2=0.10; GC_1 and GC_2 are characteristic GC, GC_1= 17%, GC_2= 90%.

Cohesion in gravelly soils is mainly composed of two parts, one is the real cohesion formed by the bonds among fine particles in the soil, and the other is the apparent cohesion formed by the occlusion among particles. With the increase of GC, the real cohesion will decrease, while the apparent cohesion will increase. When GC is low (< 40%), the rate of apparent cohesion increment is greater than the rate of real cohesion decreases. Hence, the cohesion shows an increasing trend. When GC is medium (40% - 80%), the increase rate of apparent cohesion approximately equals to the decrease rate of real cohesion, so the cohesion is stable. When GC is high (> 80%), the rate of apparent cohesion increment is increases greater than the rate of real cohesion decrement, so the cohesion shows an increasing trend again.

6. Conclusions

In this paper, a new DEM for gravelly soils is proposed based on the results of laboratory direct shear test. The reliability of this method is verified by comparing the numerical test results with the laboratory test results. Then, the shear mechanical properties and failure mechanism of gravelly soils with different GCs are studied. The main conclusions are as follows:

- During the shear process, the interaction among particles is observed, including occlusion, sliding, climbing, rotation and breakage, which affects the mechanical property and failure characteristics of gravelly soils. The shear stress-strain curves experiences three stages: rapid stress rise stage, yield stage and residual stress stage. The volumetric strain-shear strain curves first experience shear contraction and then gradually transform into shear dilation. With an increment in GC, the shear stress becomes more fluctuating, the volumetric strain tends to dilate, and the stress drop from peak stress to residual stress increases,

which can be attributed to the occlusion, squeeze and breakage of gravel particles.

- With the increase in shear strain, the contact force distribution in the sample gradually changes from uniform to uneven, and the principal stress rotates against the shear direction. Due to the interaction among particles, higher GC will increase both the average particle contact force and the force drop from peak contact force to residual force.
- The cracks first appear at the dislocation position of the shear box and then develop near the preset shear plane, which follows a speed of "slow" - "fast" - "slow". With the increase in GC, the cumulative number of cracks will increase and the shear plane of the failure sample will become coarser.
- The energy conversion can be divided into three typical stages: approximate elastic deformation stage, elastoplastic deformation stage and approximate plastic deformation stage. At the elastoplastic deformation stage, the total energy is mainly converted into the elastic strain energy. With the development of shear strain, proportions of both friction energy and breakage energy increase continuously, while proportion of elastic strain energy decreases gradually, which indicates the gradual failure of the gravelly soils.
- GC has a significant effect on the peak shear stress and strength parameters. Higher GC will change the friction angle with a trend of "stability", "increase", and "stability", while affects the cohesion with a law of "increase", "stability" and "increase".

Acknowledgments

The research described in this paper was financially supported by the National Natural Science Foundation of China (No. 51808083), the China Postdoctoral Science Foundation (No. 2020M673110) , the Basic Research and Frontier Exploration Project of Chongqing of China (No. cstc2018jcyjAX0491), the Science and Technology Research Program of Chongqing Municipal Education Commission (No. KJQN201800713), the Opening Foundation of State Key Laboratory of Mountain Bridge and Tunnel Engineering (SKLBT-19-011) and the Opening Foundation of Shaanxi Key Laboratory of Geotechnical and Underground Space Engineering (No. YT201904).

References

Afifipour, M. and Moarefvand, P. (2014a), "Failure patterns of geomaterials with block-in-matrix texture: experimental and numerical evaluation", *Arabian J. Geosci.*, **7**(7), 2781-2792. https://doi.org/10.1007/s12517-013-0907-4.

Afifipour, M. and Moarefvand, P. (2014b), "Mechanical behavior of bimrocks having high rock block proportion", *Int. J. Rock Mech. Min.*, **65**, 40-48. https://doi.org/10.1016/j.ijrmms.2013.11.008.

Bahaaddini, M. (2017), "Effect of boundary condition on the shear behaviour of rock joints in the direct shear test", *Rock Mech. Rock Eng.*, **50**(5), 1141-1155. https://doi.org/10.1007/s00603-016-1157-z.

Ben, N.O. and Einav, I. (2010), "The role of self-organization during confined comminution of granular materials", *Philos. T. R. Soc. A*, **36**(8), 231-247. https://doi.org/10.1098/rsta.2009.0205.

Bolton, M.D., Nakata, Y. and Cheng, Y.P. (2008), "Micro-and macro-mechanical behaviour of DEM crushable materials", *Géotechnique*, **58**(6), 471-480. https://doi.org/10.1680/geot.2008.58.6.471.

Bono, J. and Mcdowell, G.R. (2013), "On the micro mechanics of one-dimensional normal compression", *Géotechnique*, **63**(11), 895-908. https://doi.org/10.1680/geot.12.p.041.

Cen, D.F., Huang, D. and Ren, F. (2017), "Shear deformation and strength of the interphase between the soil–rock mixture and the benched bedrock slope surface", *Acta Geotechnica*, **12**(2), 391-413. https://doi.org/10.1007/s11440-016-0468-2.

Chang, W.J., Chang, C.W. and Zeng, J.K. (2014), "Liquefaction characteristics of gap-graded gravelly soils in K_0 condition", *Soil Dyn. Earthq. Eng.*, **56**, 74-85. http://doi.org/10.1016/j.soildyn.2013.10.005.

Chang, W.J. and Phantachang, T. (2016a), "Effects of gravel content on shear resistance of gravelly soils", *Eng Geol*, **207**, 78-90. http://doi.org/10.1016/j.enggeo.2016.04.015.

Chang, W.J., Phantachang, T. and Ieong, W.M. (2016b), "Evaluation of size and boundary effects in simple shear tests with distinct element modeling", *J. Geoeng.*, **11**(3), 133-142. http://doi.org/10.6310/jog.2016.11(3).3.

Chang, W.J. and Chou, S.H. (2019), "Experimental study on shakedown compression of saturated granular soils due to pore pressure variation", *J. Geoeng.*, **14**(4), 247-257. https://doi.org/10.6310/jog.201912_14(4).4.

Chang, W.J., Chou, S.H., Huang, H.P. and Chao, C.Y. (2021), "Development and verification of coupled hydro-mechanical analysis for rainfall-induced shallow landslides", *Eng. Geol.*, **293**(1), 106337. https://doi.org/10.1016/j.enggeo.2021.106337.

Chen, J., Gao, R., Liu, Y., Shi, Z. and Zhang, R. (2021), "Numerical exploration of the behavior of coal-fouled ballast subjected to direct shear test", *Constr. Build. Mater.*, **273**, 121927. https://doi.org/10.1016/j.conbuildmat.2020.121927.

Cheng, Y.P. and Minh, N.H. (2009), "DEM investigation of particle size distribution effect on direct shear behaviour of granular agglomerates", *Proceedings of the 6 International Conference on Micromechanics of Granular Media*, American, June.

Cho, N.A., Martin, C.D. and Sego, D.C. (2007), "A clumped particle model for rock", *Int. J. Rock Mech. Min. Sci.*, **44**(7), 997-1010. https://doi.org/10.1016/j.ijrmms.2007.02.002.

Coli, N., Berry, P., Boldini, D. and Bruno, R. (2012), "The contribution of geostatistics to the characterisation of some bimrock properties", *Eng. Geol.*, **137-138**, 53-63. https://doi.org/10.1016/j.enggeo.2012.03.015.

Danesh, A., Mirghasemi, A.A. and Palassi, M. (2020), "Evaluation of particle shape on direct shear mechanical behavior of ballast assembly using discrete element method (DEM)", *Transportation Geotechnics*, **23**, 100357. https://doi.org/10.1016/j.trgeo.2020.100357.

Einav, I. (2007), "Breakage mechanics-Part I: Theory", *J. Mech. Phys. Solids*, **55**, 1274-1297. https://doi.org/10.1016/j.jmps.2006.11.003.

Eliadorani, A., Fannin, R.J. and Wilkinson, J.M.T. (2005), "Shear strength of cohesionless soils at low stress", *Geotechnique*, **55**(6), 467-478. https://doi.org/10.1680/geot.2005.55.6.467.

Gong, H., Song, W., Huang, B., Shu, X., Han, B., Wu, H. and Zou, J. (2019), "Direct shear properties of railway ballast mixed with tire derived aggregates: Experimental and numerical investigations", *Constr. Build. Mater.*, **200**, 465-473. https://doi.org/10.1016/j.conbuildmat.2018.11.284.

Graziani, A., Rossini, C. and Rotonda, T. (2012), "Characterization and DEM modeling of shear zones at a large dam foundation", *Int. J. Geomech.*, **12**(6), 648-664. https://doi.org/10.1061/(ASCE)GM.1943-5622.0000220.

Guo, Y., Ji, Y., Zhou, Q., Markine, V. and Jing, G. (2020), "Discrete element modelling of rubber-protected ballast performance subjected to direct shear test and cyclic loading", *Sustainability*, **12**(7), 2836. https://doi.org/10.3390/su12072836

Hardin, B.O. (1985), "Crushing of soil particles", *J. Geotech. Eng.*, **111**(10), 1177-1192. https://doi.org/10.1061/(asce)0733-9410(1985)111:10(1177).

Hartl, J. and Ooi, J.Y. (2011), "Numerical investigation of particle shape and particle friction on limiting bulk friction in direct shear tests and comparison with experiments", *Powder Technol.*, **212**(1), 231-239. https://doi.org/10.1016/j.powtec.2011.05.022.

Huang, M., Xu, C.S, Zhan, J.W and Wang, J.B. (2017), "Comparative study on dynamic properties of argillaceous siltstone and its grouting-reinforced body", *Geomech. Eng.*, **13**(2), 333-352. https://doi.org/10.12989/gae.2017.13.2.333.

Huang, Y.H., Yang, S.Q., Tian, W.L. and Wu, S.Y. (2022), "Experimental and DEM study on failure behavior and stress distribution of flawed sandstone specimens under uniaxial compression", *Theor. Appl. Fract. Mech.*, **118**, 103266. https://doi.org/10.1016/j.tafmec.2022.103266.

Indraratna, B. and Salim, W. (2002), "Modelling of particle breakage of coarse aggregates incorporating strength and dilatancy", *Proceedings of the Ice-Geotechnical Engineering*, **155**(4), 243-252. https://doi.org/10.1680/geng.155.4.243.38691.

Indraratna, B., Thakur, P.K. and Vinod, J.S. (2012), "Semiempirical cyclic densification model for ballast incorporating particle breakage", *Int. J. Geomech.*, **12**(3), 260-271. https://doi.org/10.1061/(asce)gm.1943-5622.0000135.

Indraratna, B., Ngo, T. and Rujikiatkamjorn, C. (2020), "Performance of ballast influenced by deformation and degradation: laboratory testing and numerical modeling", *Int. J. Geomech.*, **20**(1), 04019138. https://doi.org/10.1061/(ASCE)GM.1943-5622.0001515.

Jiang, S., Li, X., Tan, Y., Liu, H., Xu, Z. and Chen, R. (2017), "Discrete element simulation of SiC ceramic with pre-existing random flaws under uniaxial compression", *Ceramics Int.*, **43**(16), 13717-13728. https://doi.org/10.1016/j.ceramint.2017.07.084.

Jiang, Y., Wang, L., Wu, Q., Sun, Z., Elmo, D. and Zheng, L. (2019), "An improved shear stress monitoring method in numerical direct shear tests by particle flow code", *J. Test. Evaluation*, **48**(6), 4136-4152. https://doi.org/10.1520/JTE20180018.

Jin, L., Zeng, Y.Z., Xia, L. and Ye, Y (2017), "Experimental and numerical investigation of mechanical behaviors of cemented soil–rock mixture", *Geotech. Geol. Eng.*, **35**(1), 337-354. https://doi.org/10.1007/s10706-016-0109-4.

Jing, G.Q., Ji, Y.M., Qiang, W.L. and Zhang, R. (2020), "Experimental and numerical study on ballast flakiness and elongation index by direct shear test", *Int. J. Geomech.*, **20**(10), 04020169. https://doi.org/10.1061/(ASCE)GM.1943-5622.0001791.

Kalender, A., Sonmez, H., Medley, E., Tunusluoglu, C. and Kasapoglu, K.E. (2014), "An approach to predicting the overall strengths of unwelded bimrocks and bimsoils", *Eng. Geol.*, **183**, 65-79. http://doi.org/10.1016/j.enggeo.2014.10.007.

Kamani, M. and Ajalloeian, R. (2020), "The effect of rock crusher and rock type on the aggregate shape", *Constr. Build. Mater.*, **230**(10), 1-13. https://doi.org/10.1016/j.conbuildmat.2019.117016.

Kang, D.H., Choo, J. and Yun, T.S. (2013), "Evolution of pore characteristics in the 3D numerical direct shear test", *Comput. Geotech.*, **49**, 53-61. https://doi.org/10.1016/j.compgeo.2012.10.009.

Katagiri, J., Matsushima, T. and Yamada, Y. (2010), "Simple shear simulation of 3D irregularly-shaped particles by image-based DEM", *Granular Matter*, **12**(5), 491-497. https://doi.org/10.1007/s10035-010-0207-6.

Kodicherla, S.P.K., Gong, G., Yang, Z.X., Krabbenhoft, K., Fan, L., Moy, C.K. and Wilkinson, S. (2019), "The influence of particle elongations on direct shear behaviour of granular materials using DEM", *Granular Matter.*, **21**(4), 1-12. https://doi.org/10.1007/s10035-019-0947-x.

Lee, H. and Jeon, S. (2011), "An experimental and numerical study of fracture coalescence in pre-cracked specimens under uniaxial compression", *Int. J. Solid. Struct.*, **48**(6), 979-999. https://doi.org/10.1016/j.ijsolstr.2010.12.001.

Li, C.S., Zhang, D., Du, S.S. and Shi, B. (2016), "Computed tomography based numerical simulation for triaxial test of soil–rock mixture", *Comput. Geotech.*, **73**, 179-188. https://doi.org/10.1016/j.compgeo.2015.12.005.

Lindquist, E.S. (1994), "The strength and deformation properties of melange", Ph.D. Dissertation, *University of California*, California.

Liu, G., Rong, G., Peng, J. and Zhou, C. (2015), "Numerical simulation on undrained triaxial behavior of saturated soil by a fluid coupled-DEM model", *Eng. Geol.*, **193**(2), 256-266. https://doi.org/10.1016/j.enggeo.2015.04.019.

Lobo-Guerrero, S. and Vallejo, L.E. (2005), "Discrete element method evaluation of granular crushing under direct shear test conditions", *J. Geotech. Geoenviron. Eng.*, **131**(10), 1295-1300. https://doi.org/10.1061/(ASCE)1090-0241(2005)131:10(1295).

Medley, E.W. (1994), "The engineering characterization of melanges and similar block-in-matrix rocks (Bimrocks)", Ph.D. Dissertation, *University of California at Berkeley*, California.

Ngo, N.T., Indraratna, B. and C. Rujikiatkamjorn. (2016), "Modelling geogrid-reinforced railway ballast using the discrete element method", *Transp. Geotech.*, **8**, 86-102. https://doi.org/10.1016/j.trgeo.2016.04.005.

Rahmani, H. and Panah, A.K. (2020), "Effect of particle size and saturation conditions on the breakage factor of weak rockfill materials under one-dimensional compression testing", *Geomech. Eng.*, **21**(4), 315-326. http://dx.doi.org/10.12989/gae.2020.21.4.315.

Salazar, A., Sáez, E. and Pardo, G. (2015), "Modeling the direct shear test of a coarse sand using the 3D Discrete Element Method with a rolling friction model", *Comput. Geotech.*, **67**, 83-93. https://doi.org/10.1016/j.compgeo.2015.02.017.

Seyyedan, S.M., Mirghasemi, A.A. and Mohammadi, S. (2021), "Numerical simulation of direct shear test on granular materials composed of breakable angular particles: A DEM-XFEM approach", *Powder Technol.*, **391**, 450-466. https://doi.org/10.1016/j.powtec.2021.06.038.

Shahnazari, H. and Rezvani, R. (2013), "Effective parameters for the particle breakage of calcareous sands: An experimental study", *Eng. Geol.*, **159**(9), 98-105. http://doi.org/10.1016/j.enggeo.2013.03.005.

Shinohara, K., Oida, M. and Golman, B. (2000), "Effect of particle shape on angle of internal friction by triaxial compression test", *Powder Technol.*, **107**(1-2), 131-136. https://doi.org/10.1016/S0032-5910(99)00179-5.

Song, Z.P., Li, S.H., Wang, J.B., Sun, Z.Y. and Liu, J. (2018), "Determination of equivalent blasting load considering millisecond delay effect", *Geomech. Eng.*, **15**(2), 745-754. https://doi.org/10.12989/gae.2018.15.2.745.

Sonmez, H., Gokceoglu, C., Mendly, E.W., Tuncay, E. and Nefeslioglu, H.A. (2006), "Estimating the uniaxial compressive strength of a volcanic bimrock", *Int. J. Rock Mech. Min.*, **43**(4), 554-561. https://doi.org/10.1016/j.ijrmms.2005.09.014.

Sonmez, H., Ercanoglu, M., Kalender, A., Dagdelenler, G. and

Tunusluoglu, C. (2016), "Predicting uniaxial compressive strength and deformation modulus of volcanic bimrock considering engineering dimension", *Int. J. Rock Mech. Min.*, **86**, 91-103. http://doi.org/10.1016/j.ijrmms.2016.03.022.

Suhr, B., Marschnig, S. and Six, K. (2018), "Comparison of two different types of railway ballast in compression and direct shear tests: experimental results and DEM model validation", *Granular Matter.*, **20**(4), 1-13. https://doi.org/10.1007/s10035-018-0843-9.

Tsoungui, O., Vallet, D. and Charmet, J.C. (1999), "Numerical model of crushing of grains inside two-dimensional granular materials", *Powder Technol.*, **105**(1-3), 190-198. https://doi.org/10.1016/s0032-5910(99)00137-0.

Tu, Y.L., Chai, H.J., Liu, X.R., Wang, J.B. and Yu, J.Y. (2021), "An experimental investigation on the particle breakage and strength properties of soil-rock mixture", *Arabian J. Geosci.*, **14**, 840. https://doi.org/10.1007/s12517-021-07186-0.

Wang, J.B, Zhang, Q., Song, Z.P. and Zhang, Y.W. (2020), "Creep properties and damage constitutive model of salt rock under uniaxial compression", *Int. J. Damage Mech.*, **29**(6), 902–922. https://doi: 10.1177/1056789519891768.

Wang, Y., Li, C.H. and Hu, Y.Z. (2018), "Use of X-ray computed tomography to investigate the effect of rock blocks on meso-structural changes in soil-rock mixture under triaxial deformation", *Constr. Build. Mater.*, **164**, 386-399. https://doi.org/10.1016/j.conbuildmat.2017.12.173.

Xiao, J., Zhang, D., Wei, K. and Luo, Z. (2017), "Shakedown behaviors of railway ballast under cyclic loading", *Constr. Build. Mater.*, **155**, 1206-1214. https://doi.org/10.1016/j.conbuildmat.2017.07.225.

Xu, W.J., Xu, Q. and Hu, R.L. (2011), "Study on the shear strength of soil–rock mixture by large scale direct shear test", *Int. J. Rock Mech. Min. Sci.*, **48**(8), 1235-1247. https://doi.org/10.1016/j.ijrmms.2011.09.018.

Xu, W.J., Li, C.Q. and Zhang, H.Y. (2015), "DEM analyses of the mechanical behavior of soil and soil-rock mixture via the 3D direct shear test", *Geomech. Eng.*, **9**(6), 815-827. http://dx.doi.org/10.12989/gae.2015.9.6.815.

Xu, W.J., Wang, S., Zhang, H.Y. and Zhang, Z.L. (2016), "Discrete element modelling of a soil-rock mixture used in an embankment dam", *Int. J. Rock Mech. Min. Sci.*, **86**, 141-156. https://doi.org/10.1016/j.ijrmms.2016.04.004.

Xu, D.S., Tang, J.Y. and Zou, Y. (2019), "Macro and micro investigation of gravel content on simple shear behavior of sand-gravel mixture", *Constr. Build. Mater.*, **221**, 730-744. https://doi.org/10.1016/j.conbuildmat.2019.06.091.

Zhang S., Tang H.M., Zhang H.B., Lei G.P. and Cheng H (2015), "Investigation of scale effect of numerical unconfined compression strengths of virtual colluvial-deluvial soil-rock mixture". *Int. J. Rock Mech. Min.*, **77**, 208-219. http://doi.org/10.1016/j.ijrmms.2015.04.012.

Zhang, S. (2015), "Soil-rock mixture slope deformation behavior study based on structuredness", Ph.D. thesis, *China University of Geosciences*.

Zhang, Z.L., Xu, W.J., Xia, W. and Zhang, H.Y. (2016), "Large-scale in-situ test for mechanical characterization of soil–rock mixture used in an embankment dam", *Int. J. Rock Mech. Min. Sci.*, **86**, 317-322. https://doi.org/10.1016/j.ijrmms.2015.04.001.

Zhang, Z., Cui, Y., Chan, D.H. and Taslagyan, K.A. (2018), "DEM simulation of shear vibrational fluidization of granular material", *Granular Matter.*, **20**(71), 141-156. https://doi.org/10.1007/s10035-018-0844-8.

Zhang, N., Hedayat, A., Bolaños Sosa, H.G., González Cárdenas, J.J., Salas Alvarez, G.E., Rivera, V.A. and González, J. (2020), "Fracture and failure processes of geopolymerized mine tailings under uniaxial compression", *Proceedings of the* 54th US Rock Mechanics/Geomechanics Symposium. American, June.

Zhou, Z., Yang, H., Xing, K. and Gao, W. (2018), "Prediction models of the shear modulus of normal or frozen soil-rock mixtures", *Geomech. Eng.*, **15**(2), 783-791. http://dx.doi.org/10.12989/gae.2018.15.2.783.

IC